



# Influence of La<sup>3+</sup> ions doping on morphology and magnetic properties of Mg–Co ferrites

Xiaoyan Huang<sup>1</sup> · Aimin Sun<sup>1,2</sup> · Ying Jiang<sup>1</sup> · Jialing Wang<sup>1</sup> · Yanchun Zhang<sup>1</sup> · Liqiong Shao<sup>1</sup>

Received: 12 July 2021 / Accepted: 30 October 2021 / Published online: 19 November 2021  
© The Author(s), under exclusive licence to Springer-Verlag GmbH, DE part of Springer Nature 2021

## Abstract

In this study, magnesium–cobalt nanoferrites (MCNF) doped with La<sup>3+</sup> ions were prepared by sol–gel method. The chemical formula of the samples prepared was Mg<sub>0.2</sub>Co<sub>0.8</sub>Fe<sub>2-x</sub>La<sub>x</sub>O<sub>4</sub> (x = 0.0, x = 0.025, x = 0.05, x = 0.075, x = 0.1). The crystal structure of the samples and the successful doping of La<sup>3+</sup> ions can be obtained by X-ray diffraction (XRD). Fourier transform infrared spectroscopy (FTIR) reflects the information of absorption bands and functional groups in a certain range. According to the position of different absorption bands, it can be judged that the chemical reaction has been completed in the preparation process. Scanning electron microscopy (SEM) images showed that the sample is spherical, the particle size distribution is narrow, and the sample size is uniform. Energy dispersion spectroscopy (EDS) was used to characterize the specific elements in the samples and confirmed that the elements in the samples were Mg, Co, Fe, La, and O. There were no other impurities in the samples. Vibrating sample magnetometer (VSM) is used primarily to analyze the magnetic properties of samples. The results demonstrate that the doping of La<sup>3+</sup> ions can change the crystal properties of the samples, and Mg<sub>0.2</sub>Co<sub>0.8</sub>Fe<sub>2-x</sub>La<sub>x</sub>O<sub>4</sub> has a cubic spinel structure. The coercivity of the sample is between 611.24 and 779.43 Oe, and it has the properties of hard magnetic materials.

**Keywords** Magnesium–cobalt nanoferrites (MCNF) · La<sup>3+</sup> ions doping · Sol–gel · Structural · Magnetic properties

## 1 Introduction

Ferrites are representative oxides of ferromagnetic materials. Their main compositions are iron oxides, sometimes doped with rare earth elements. [1, 2]. Most ferrites belong to semiconductor, and their resistivities are much higher than those general metallic magnetic materials. They have the advantage of small eddy current loss. Ferrites have wide ranges of applications; they can be used in biomedicine, magnetic storage media, catalysts, radio energy transmission systems and environmental governance [3, 4]. In recent years, compared with bulk materials, nanomaterials have become the focus of many researchers because of their unique applications [5]. Ferrite nanomagnetic materials have smaller quantum

sizes, and they have surface and macroscopic quantum tunneling effects; therefore, ferrite nanomagnetic materials have attracted extensive attention of scientists [6, 7].

Among all kinds of spinel ferrites, cobalt nanoferrites (CNF) have attracted much attention because of their high saturation magnetization, high coercivity and strong anisotropy constant. Doping or substituting cations in the lattice of spinel will change the physical and chemical properties of CNF [8–10]. In particular, the study of Mg<sup>2+</sup>-doped CNF shows that the saturation magnetization, magnetostrictive energy and anisotropy constant of CNF are reduced by replacing Co<sup>2+</sup> with Mg<sup>2+</sup> [11]. Rare-earth elements (RE) have typical relaxation characteristics. Since the doping of rare-earth ions provides good conditions for the vacancy and gap in the spinel ferrites, the composite oxides with different spinel structures can be prepared. The ferrites doped with rare-earth ions have the characteristics of high magnetic permeability, high saturation magnetization and low coercivity, and these ferrites have wider ranges of applications [12]. However, the synthesis of Mg–Co ferrite doped with La<sup>3+</sup> ions has not been reported.

✉ Aimin Sun  
sunam@nwnu.edu.cn

<sup>1</sup> College of Physics and Electronic Engineering, Northwest Normal University, Lanzhou 730070, China

<sup>2</sup> Key Laboratory of Atomic and Molecular Physics & Functional Materials of Gansu Province, Lanzhou 730070, China

According to their structure, ferrite can be divided into spinel, garnet, perovskite and magnetic lead stone, etc. According to the application, it can be divided into hard magnetic, soft magnetic, permanent magnetic, moment magnetic and other types [13–16]. The methods of preparing ferrite nanometer magnetic materials include sol–gel method, chemical co-precipitation method, hydrothermal method, microwave-assisted method and high-temperature decomposition method, among them the sol–gel method is simpler and cheaper than other methods [17].

In this experiment, magnesium–cobalt nanoferrites (MCNF) doped with  $\text{La}^{3+}$  were prepared by sol–gel method. The doping amount increases from 0 to 0.1 at an interval of 0.025. The main purpose of this study is to change the magnetic properties of Mg–Co ferrite and then apply it to microwave absorption materials.

## 2 Experimental process

In this study, MCNF doped with  $\text{La}^{3+}$  ions were prepared by sol–gel method, and the chemical formula of the sample prepared was  $\text{Mg}_{0.2}\text{Co}_{0.8}\text{Fe}_{2-x}\text{La}_x\text{O}_4$  [10, 18].

### 2.1 Experimental materials

The metal nitrates used in the experiment are magnesium nitrate ( $\text{Mg}(\text{NO}_3)_2 \cdot 6\text{H}_2\text{O}$ ), cobalt nitrate ( $\text{Co}(\text{NO}_3)_2 \cdot 6\text{H}_2\text{O}$ ), ferric nitrate ( $\text{Fe}(\text{NO}_3)_3 \cdot 9\text{H}_2\text{O}$ ) and lanthanum nitrate ( $\text{La}(\text{NO}_3)_3 \cdot 6\text{H}_2\text{O}$ ). The complexing agent was citric acid ( $\text{C}_6\text{H}_8\text{O}_7$ ). The function of citric acid is to fully merge the metal cations in the solution.

### 2.2 Preparatory work

Clean the beaker with deionized water and alcohol and then air dry. Set the electronic scale to zero, then place the weighing paper on the electronic scale and set the scale to zero again. Weighing out the required quality of metal nitrate. The molar amount of citric acid is 1.2 times that of metal nitrates. Place the metal nitrates and citric acid in a cleaned beaker and then add 100 ml of deionized water.

### 2.3 Sol–gel process

Firstly, stir thoroughly with a clean glass rod until the metal nitrates and citric acid have dissolved. Secondly, drop ammonia water ( $\text{NH}_3 \cdot \text{H}_2\text{O}$ ) to the completely dissolved solution. During dropping process, the glass rod was continuously stirred to adjust the pH value of the solution to 7. The final solution was rouge black. The prepared solution is referred to as the precursor solution. Lastly, put the small magnetic needle into the beaker and stir the solution in a

magnetic stirrer with a constant temperature at  $80^\circ\text{C}$ . After this process lasts for 2–3 h, a wet gel is obtained. Place the obtained wet gel in a blast furnace at  $120^\circ\text{C}$  to dry for 2 h.

### 2.4 Annealing and grinding

The dried sample was burned with an alcohol blowtorch to obtain a silver-gray flocculent. Put the flocculent in a mortar and grind it for about 40 min to get a powder. Place the powder in a magnetic boat and sintered in a tube furnace at  $950^\circ\text{C}$  for 3 h and then grind it in an agate bowl for half an hour to get the final product. Figure 1 shows the specific experimental flow.

## 3 Results and discussion

### 3.1 Structural characterization

A ferrite cell contains 56 ions, of which 8 are metal ions, 16 are trivalent iron ions and 32 are oxygen ions. Of the

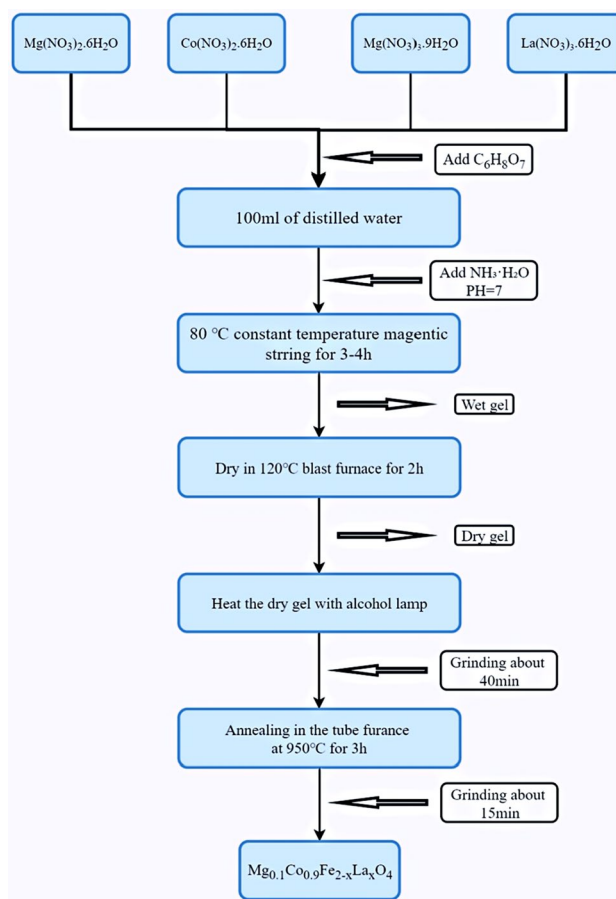


**Fig. 1** Flow chart for the synthesis of  $\text{Mg}_{0.2}\text{Co}_{0.8}\text{Fe}_{2-x}\text{La}_x\text{O}_4$  ( $x=0, 0.025, 0.05, 0.075, 0.1$ ) nanoferrite particles by sol gel auto combustion process

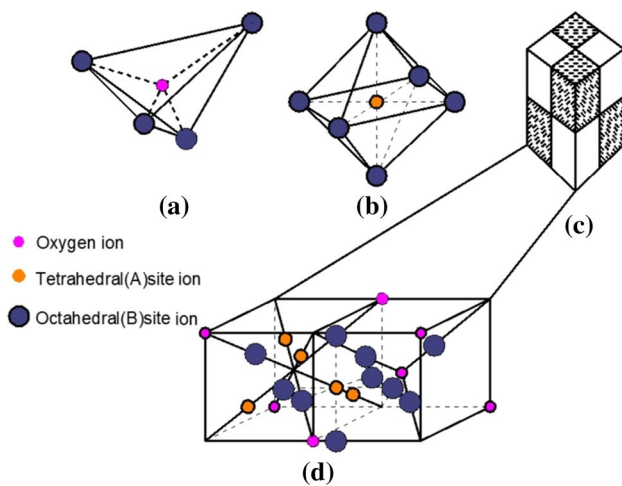


**Fig. 2** a–d The crystal structure of spinel ferrite. **a** tetrahedral A site; **b** octahedral B site; **d** the distribution of metal cations and oxygen ions

three types of ions contained in ferrite cells, oxygen ions are the largest. Therefore, the lattice composition of ferrite is: oxygen ions do dense accumulation, and metal ions fill the gaps between the dense accumulation of oxygen ions [19–21]. Figure 2 shows the crystal cell structure of spinel-type ferrites. In the face-centered cubic crystal composed of 32 oxygen ions packed closely, there are two kinds of gaps, tetrahedral gaps and octahedral gaps. The tetrahedral gaps are surrounded by four triangular planes formed by the central connecting lines of four oxygen ions, and there are 64 such gaps [22]. Tetrahedron gaps are small, and they can only fill the small sizes of metal ions. The octahedral gaps are surrounded by 8 triangular planes consisting of 6 oxygen ions' central connecting lines, and there are 32 such gaps. The octahedron has a large gap and can be filled with large metal ions. The tetrahedral gaps are called the A sites and the octahedral gaps are called the B sites. The occupancies of different ions in the crystal lattice are mainly affected by the following aspects: (I) Ions with large radius tend to occupy B sites. (ii) Due to the high electronegativity of B site, high-priced ions with higher charge are more likely to occupy B sites. (iii) In general, metal ions that can form sp<sup>3</sup> hybrid orbitals tend to occupy A sites. (IV) The lattice electric field energy at B site is lower. (V) Metal ion replacement will change the original ion distribution. (VI) Under the condition of high temperature, due to thermal turmoil, some metal ions will change their original occupancies and tend to be evenly distributed in the A and B sites [23–25].

Figure 3 shows the XRD patterns of MCNF with different doping amounts of La<sup>3+</sup> ions. It can be seen from the figure that the diffraction peaks of samples without La<sup>3+</sup> ions doping and with different doping amounts are consistent with the standard spectrum diffraction peaks

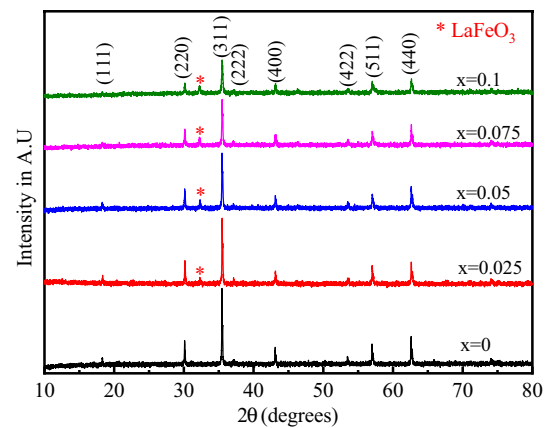


**Fig. 3** X-ray powder diffraction for Mg<sub>0.2</sub>Co<sub>0.8</sub>La<sub>x</sub>Fe<sub>2-x</sub>O<sub>4</sub> (x = 0, 0.025, 0.05, 0.075, 0.1) nanoferrite particles

of cubic spinel structure. It shows that MCNF with spinel structure has been prepared. However, when doping amount  $x = 0.025$  or higher, a small impurity peak appears at around 35 degrees. This peak corresponds to FeLaO<sub>3</sub>, which called external phase. The cause of the external phase is that the virtual melt is re-formed at the solid–solid interface during sample preparation [26]. That is to say, the change of lattice shape caused by doping leads to phase transformation behavior, which induces different scale effects [27]. The cause of the external phase also indicates that the solubility of La<sup>3+</sup> ions in this kind of ferrite is low, and parts of La<sup>3+</sup> ions in the samples are not doped successfully.

According to the measured XRD patterns and the theoretical calculation formula, some important parameters about the structural characteristics of the samples can be obtained. Specific data values are shown in Table 1.

The formula are as follows:

$$a = d\sqrt{h^2 + k^2 + l^2} \quad (1)$$

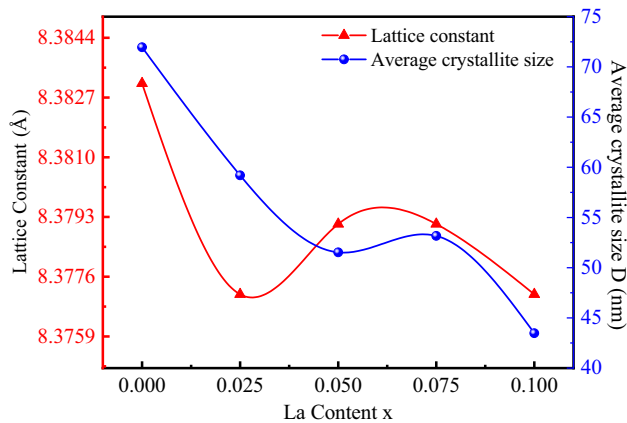
where 'a' is the lattice constant, (h, k, l) is the Miller exponent representing the direction of the crystal plane, and 'd' is the plane spacing between two crystal faces in the crystal. The lattice constant of the samples with different doping amount can be calculated by this formula [28].

$$D = \frac{0.9\lambda}{\beta \cos \theta} \quad (2)$$

From this formula, the average size of the crystal 'D' can be calculated, where 'λ' represents the wavelength of the X-ray, 'β' represents the full width of the half peak of the diffraction peak, and 'θ' represents the Bragg Angle of the peak position of the main peak. This formula is known as Scherer's formula [29].

**Table 1** Parameters obtained from XRD data for  $\text{Mg}_{0.2}\text{Co}_{0.8}\text{Fe}_{2-x}\text{La}_x\text{O}_4$  ( $x=0.0, 0.025, 0.05, 0.075, 0.1$ ) nanoferrite particles

Composition, x	Inter planar spacing 'd' (Å)	Lattice constant 'a' (Å)	Crystal size 'D' (nm)	Volume of unit cell 'a <sup>3</sup> ' (Å <sup>3</sup> )	Dislocation line density 'δ' (10 <sup>-3</sup> nm <sup>-2</sup> )	X-ray density 'ρ <sub>x</sub> ' (Kg/m <sup>3</sup> )
0.0	2.5276	8.3831	71.9633	589.13	1.93	5134.22
0.025	2.5258	8.3771	59.2083	587.87	2.85	5192.90
0.05	2.5264	8.3791	51.5318	588.29	3.76	5235.49
0.075	2.5264	8.3791	53.1730	588.29	3.54	5282.24
0.1	2.5258	8.3771	43.4811	587.87	5.29	5332.79

**Fig. 4** Variation of lattice constant, average crystallite size of La content (x)

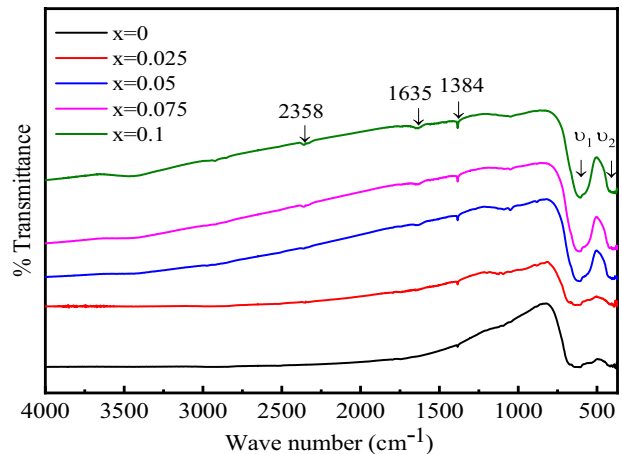
$$\delta = \frac{1}{D^2} \quad (3)$$

The dislocation line density 'δ' can be calculated by this formula [30].

$$\rho_x = \frac{8M}{N_A a^3} \quad (4)$$

The X-ray density 'ρ<sub>x</sub>' can be obtained by this equation. In this formula, 'M' is the relative molecular weight of the sample with different doping amounts. 'N<sub>A</sub>' is Avogadro constant, and its value is  $6.02 \times 10^{23}$ .

The variation of lattice constant and average grain size with  $\text{La}^{3+}$  ions contents are shown in Fig. 4. The radius of the  $\text{La}^{3+}$  (1.126 Å) is larger than that of the  $\text{Fe}^{3+}$  (0.65 Å), so this kind of change in the lattice constant is unexpected. The reason for the decrease in the lattice constant is that the radius difference between  $\text{La}^{3+}$  and  $\text{Fe}^{3+}$  ions causes the cationic rearrangement between A and B sites, which cause the local deformation of the lattice. The resulting internal stress effect causes the uneven volume displacement of the macroscopic or microscopic structures inside the material. Thus inhibiting the growth of the lattice [31].

**Fig. 5** FT-IR spectra of  $\text{Mg}_{0.2}\text{Co}_{0.8}\text{Fe}_{2-x}\text{La}_x\text{O}_4$  ( $x=0.0, 0.025, 0.05, 0.075, 0.1$ ) nanoferrite particles

It can be seen from the calculation results in Table 1 that the dislocation line density shows an increasing trend. This is because  $\text{La}^{3+}$  ions occupied the void positions in the crystal lattice, thereby increasing the grid points in the crystal [32]. The increase in the dislocation line density indicates a decrease in the crystallinity of the sample. This may be due to the low sintering temperature during sample's preparation. Therefore, the sintering temperature or sintering time should be appropriately increased to improve the crystallinity of samples. With the increase in  $\text{La}^{3+}$  ions' doping amount, the X-ray density also increases. This is because  $\text{Fe}^{3+}$  (55.85 g/mol) was replaced by  $\text{La}^{3+}$  (138.9 g/mol) with bigger mass volume ratio [33].

### 3.2 Fourier transform infrared spectroscopy (FTIR)

FTIR spectroscopic analysis can be used to identify the molecular bands associated with the attachment, and the functional group information left by chemical reagents used in the synthesis process. The FTIR spectrums of the sintered  $\text{Mg}_{0.2}\text{Co}_{0.8}\text{Fe}_{2-x}\text{La}_x\text{O}_4$  ferrite system ( $x=0.0, x=0.025, x=0.05, x=0.075, x=0.1$ ) are shown in Fig. 5. As can be seen from the figure, there are two main absorption bands in the range of  $250 \text{ cm}^{-1}$  to  $4000 \text{ cm}^{-1}$ , which

**Table 2** Frequency bands  $\nu_1$  and  $\nu_2$  of the samples

Composition, x	Sample	$\nu_1$ (cm <sup>-1</sup> )	$\nu_2$ (cm <sup>-1</sup> )
0.0	Mg <sub>0.2</sub> Co <sub>0.8</sub> Fe <sub>2</sub> O <sub>4</sub>	608	378
0.025	Mg <sub>0.2</sub> Co <sub>0.8</sub> Fe <sub>1.975</sub> La <sub>0.025</sub> O <sub>4</sub>	606	355
0.05	Mg <sub>0.2</sub> Co <sub>0.8</sub> Fe <sub>1.95</sub> La <sub>0.05</sub> O <sub>4</sub>	608	354
0.075	Mg <sub>0.2</sub> Co <sub>0.8</sub> Fe <sub>1.925</sub> La <sub>0.075</sub> O <sub>4</sub>	607	329
0.1	Mg <sub>0.2</sub> Co <sub>0.8</sub> Fe <sub>1.9</sub> La <sub>0.1</sub> O <sub>4</sub>	605	331

occur around 610 cm<sup>-1</sup> and 350 cm<sup>-1</sup> respectively. The specific values are shown in Table 2. The appearances of these two prominent absorption bands proved that the samples have spinel structures. According to Table 2, with the increase of La<sup>3+</sup> ions contents, the absorption bands move to low frequency, indicating that La<sup>3+</sup> ions replaced Fe<sup>3+</sup> ions. The bands observed at 1635 cm<sup>-1</sup> attributed to H–O–H stretching and bending patterns were interpreted as evidence of free water. The bands at 1380 cm<sup>-1</sup> may be due to the stretching vibrations of the antisymmetric NO<sup>3-</sup> and ferrite tetrahedral complexes. Besides, there are tiny absorption bands at 2358 cm<sup>-1</sup>, which represent hydrogen bonds of water molecules [34]. The absence of hydroxyl group and carboxylic group (at 3200 ~ 3700 cm<sup>-1</sup>) in sample sintered at 950 °C for 3 h reveals the completion of chemical reaction [35].

### 3.3 Scanning electron microscopy (SEM)

Figure 6a–e shows the scanning electron microscope (SEM) images of MCNF doped with different amounts of La<sup>3+</sup> ions (x = 0.0, 0.025, 0.05, 0.075, 0.1). SEM images show that the samples are spherical in the nanometer scale, with small particle sizes and uniform distributions. But due to the interaction between magnetic particles, the particles condense to form clusters to some extent. The formation of nanosize crystallites was verified by SEM images. The average particle sizes are between 16 and 25 nm. As can be seen from Fig. 6, the size distribution of the prepared sample is narrow, indicating that the samples' sizes are relatively uniform.

### 3.4 Energy dispersive spectroscopy (EDS)

As shown in Fig. 7, the elemental composition analysis of the five samples' selections was carried out with red wire frame on the SEM images to obtain the corresponding EDS images. EDS was used to confirm the elemental composition of the sample. It can be seen that with the increase in doping amount, the content of lanthanum element increases significantly, indicating that La<sup>3+</sup> ions have been doped into MCNF. The results show that the element compositions are

consistent with the formula calculation results, and there are no other impurity elements in the samples.

### 3.5 Magnetic measurements

In this experiment, the magnetic properties of the prepared samples are mainly studied. The magnetization curve is a description of the nonlinear relationship between magnetization intensity 'M' and magnetic field intensity 'H'. A closed curve is formed in the process of the external magnetic field 'H' from the positive maximum to the negative maximum and back to the positive maximum, which is called the hysteresis loop. The hysteresis loops obtained in this experiment are shown in Fig. 8. The hysteresis loops of the measured ferrite samples showed their ferromagnetic behavior. When the saturation magnetization, remanence magnetization and coercivity of ferrite are relatively high, the output capacity of information in application will be improved accordingly, so as to realize more efficient magnetic storage and magneto-optical recording functions [36]. Remanence magnetization (Mr) and saturation magnetization (M<sub>s</sub>) can be obtained through hysteresis loops, and the specific values are shown in Table 3.

The magnetism of ferrite mainly comes from the superexchange of metal cations between A and B sites. Figure 9a describes the variation of M<sub>s</sub> and Mr with La<sup>3+</sup> ions contents. As can be seen from Table 3, the M<sub>s</sub> decreased from 61.99 to 53.29 emu/g, and then increased to 54.34 emu/g at x = 0.1. The Mr increased from 26.67 to 29.33 emu/g, and then decreased slightly at x = 0.05. According to the Neel's model, the increase in M<sub>s</sub> and Mr leads to the increase in magnetic properties of the samples. This is because the doped La<sup>3+</sup> ions had two unpaired electrons and metal Co<sup>2+</sup> ions which occupied the octahedral sites had three unpaired electrons, the doped La<sup>3+</sup> ions have larger radius, they tend to occupy the B sites of the octahedron, so this increases the number of unpaired electrons in octahedral gap in MCNF, thus promoting the superexchange interaction between A sites and B sites. The reason for the decrease in magnetic properties is that the migration of Fe<sup>3+</sup> from B site to A site leads to the decrease in magnetic moment, resulting in the decrease in both M<sub>s</sub> and Mr. In addition, after doping La<sup>3+</sup> ions in MCNF, with the increase of La<sup>3+</sup> contents, the squareness S (Mr/M<sub>s</sub>) and the coercivity squareness (S\*) both show an increasing trend, but slightly decrease when x = 0.05. Squareness, also known as residual magnetization ratio, is an important parameter for ferromagnetic materials. When x = 0.1, the residual magnetization ratio S (Mr/M<sub>s</sub>) and the coercivity squareness (S\*) have the maximum values, which are 0.539 and 0.343. According to the literature [37], when the residual magnetization ratio (Mr/M<sub>s</sub>) is less than 0.6, there are cubic anisotropic single domain

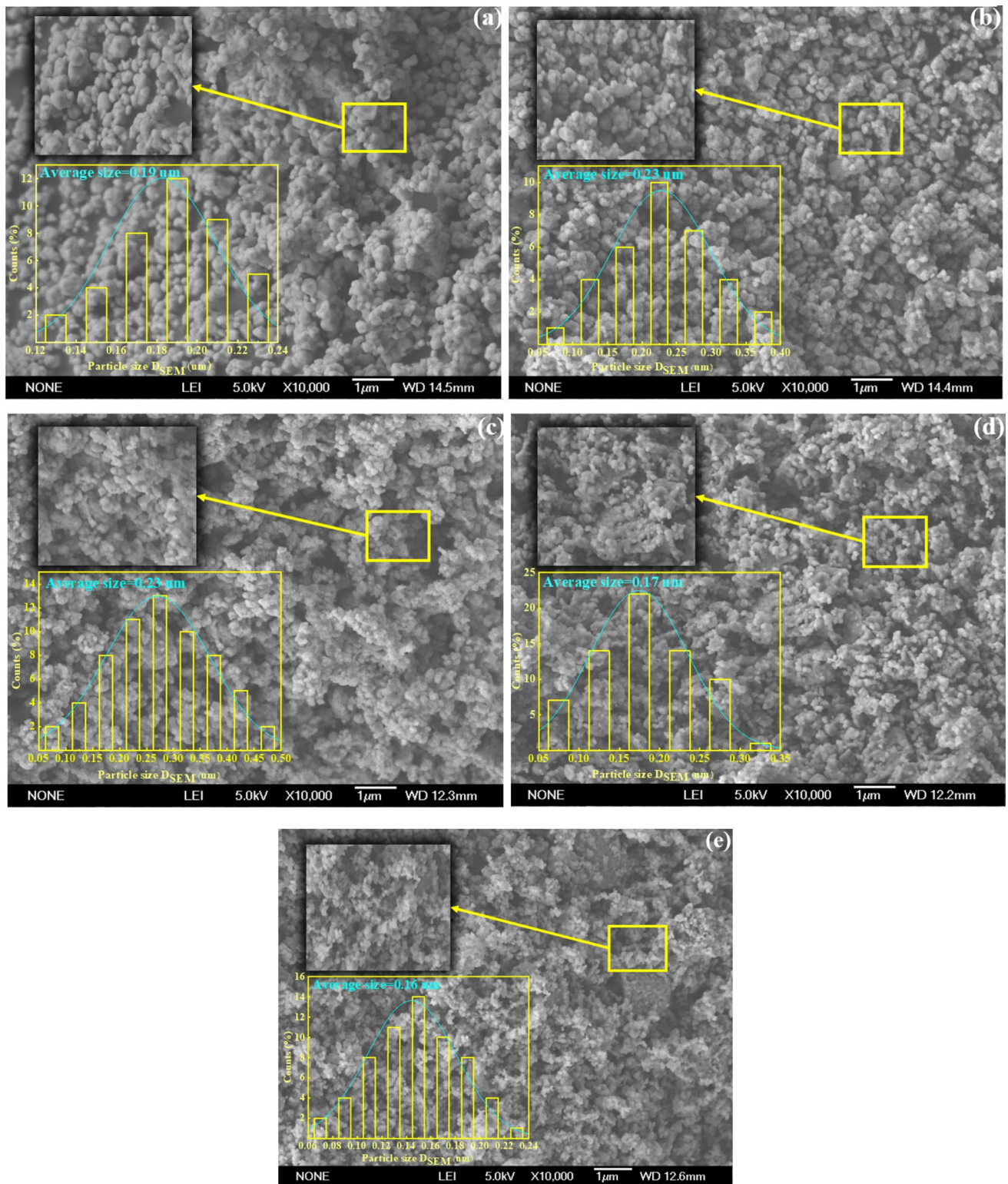


**Fig. 6** Scanning electron microscopy micrographs and the particle size distribution (obtained from SEM) of  $\text{Mg}_{0.2}\text{Co}_{0.8}\text{Fe}_{2-x}\text{La}_x\text{O}_4$  ferrite nanoparticles: **a**  $x=0.0$ , **b**  $x=0.025$ , **c**  $x=0.05$ , **d**  $x=0.075$ , **e**  $x=0.1$

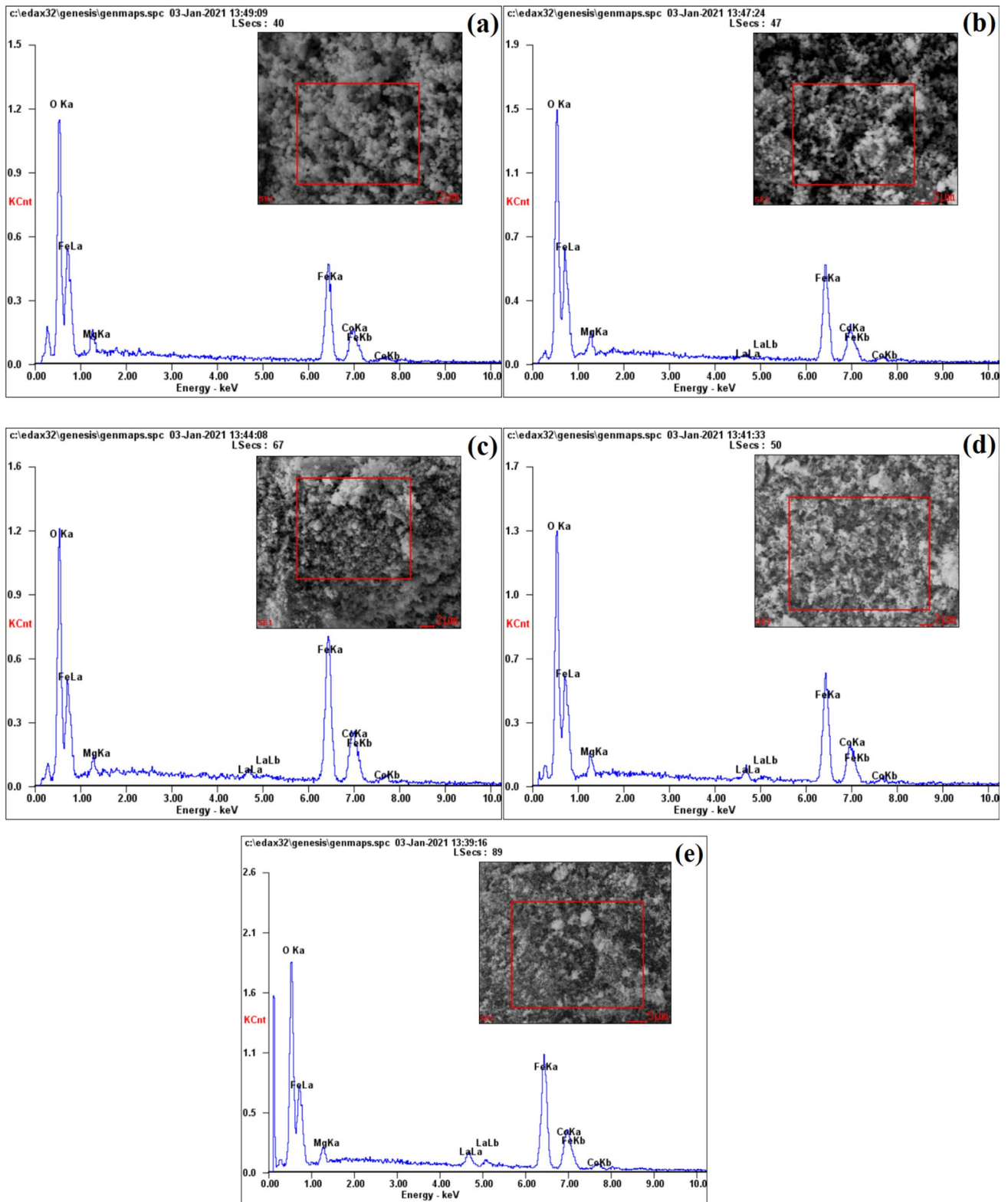


**Fig. 7** EDS spectra of  $\text{Mg}_{0.2}\text{Co}_{0.8}\text{Fe}_{2-x}\text{La}_x\text{O}_4$  ferrite nanoparticles: **a**  $x=0.0$ , **b**  $x=0.025$ , **c**  $x=0.05$ , **d**  $x=0.075$ , **e**  $x=0.1$

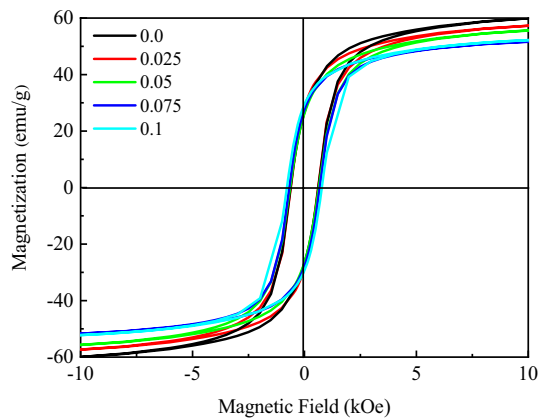


**Fig. 8** M-H hysteresis loops of  $Mg_{0.2}Co_{0.8}Fe_{2-x}La_xO_4$  ferrite system

particles in the composition of the surface samples. It can be seen that the prepared samples in this experiment are single domain particles with cubic anisotropy.

The magnetic parameters were calculated in conjunction with the data in Table 3 and the following formula, as shown in Table 4.

The theoretical magnetization of spinel ferrite can be calculated by the following equation:

$$\mu_{B(\text{Cal.})} = M_B - M_A \tag{5}$$

The ‘ $\mu_B$ ’ is the total magnetic moment. ‘ $M_A$ ’ and ‘ $M_B$ ’ are the magnetic moments of metal ions at the A and B positions [38].

$$\mu_{B(\text{exp.})} = \frac{M_W \times M_S}{5585} \tag{6}$$

The magnetic moments of each formula element in the Bohr magnet can be calculated by this formula. Where ‘ $M_W$ ’ is the molecular weight of ferrite with different doping amounts [39].

$$H_C = \frac{2K}{\mu_0 \times M_S} \tag{7}$$

The ‘ $H_c$ ’ is coercivity, ‘ $\mu_0$ ’ is vacuum permeability, ‘ $M_s$ ’ is saturation magnetization, and ‘ $K$ ’ is magnetic anisotropy constant [40].

Magnetization occurs when the magnitude of the interaction between A and B is higher than that between A-A or A-B. Therefore, the magnetic moment of the A-sublattice cancels out part of the magnetic moment of the B-sublattice, and the remaining B-sublattice is magnetized to produce net magnetic moment. Since the magnetization ( $M$ ) is different between the magnetic moments at two sites, ‘ $M$ ’ can be increased by increasing the magnetic moment at B sites or decreasing the magnetic moment at A sites [41].

The coercivity force is the magnetic field strength when the reverse magnetic field reaches a certain value, satisfying  $M=0$ . The coercivity is to characterize the ability of magnetic materials to remain magnetized, which is an important parameter of magnetic materials. Coercivity is not only one of the important criteria for reference of permanent magnetic material, but also an important basis for the division of soft magnetic materials and permanent magnetic materials.

**Table 3** Magnetic parameters of the prepared ferrite samples

Composition, x	Remanent magnetization $M_r$ (emu/g)	Saturation magnetization $M_s$ (emu/g)	Coercivity $H_c$ (Oe)	Squareness S (Mr/Ms)	Coercivity Squareness $S^*$
0.0	26.67	61.99	621.15	0.430	0.237
0.025	28.34	59.28	611.24	0.478	0.227
0.05	26.29	57.83	640.97	0.455	0.214
0.075	27.70	53.29	679.55	0.520	0.270
0.1	29.33	54.34	779.43	0.539	0.343

**Table 4** The values of magnetic moment, magnetic anisotropy,  $dM/dH$  and  $H_m$  calculated from  $M(H)$  data of  $Mg_{0.2}Co_{0.8}Fe_{2-x}La_xO_4$  ( $x=0.0, 0.025, 0.05, 0.075, 0.1$ )

Composition, x	Unit cell mag mom $\mu_{B(\text{exp.})}$	Anisotropy Constant $K \times 10^4$ (erg/g)	$H_m$ (Oe)	$dM/dH$ (emu/(g Oe)) $\times 10^{-3}$	$H \rightarrow H_m$
				$H \rightarrow 0$	$H \rightarrow H_m$
0.0	2.53	2.51	498.1	27.22	55.34
0.025	2.43	2.36	498.1	26.66	59.61
0.05	2.40	2.42	497.9	25.41	51.34
0.075	2.23	2.36	497.9	21.93	52.52
0.1	2.29	2.77	896.1	20.40	55.91



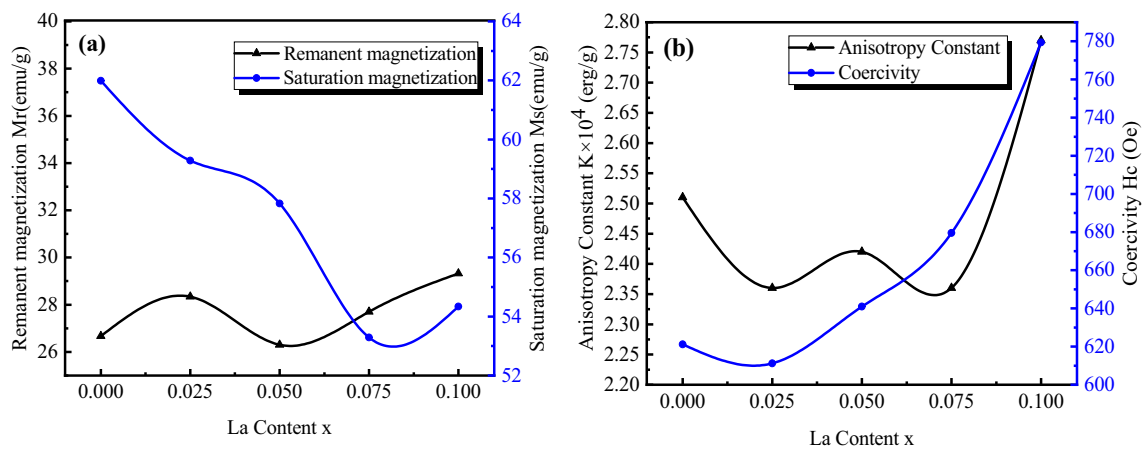


**Fig. 9** **a** Variation of saturation magnetization, remanent magnetization with La content, **b** variation of anisotropy constant and coercivity with La content

Figure 9b describes the variation of anisotropy constants and coercivity with La<sup>3+</sup> ions contents. As is shown in Table 3, the coercivity of MCNF increased with the increasing of La<sup>3+</sup> contents, but decreased slightly when  $x = 0.025$ , and the coercivity reaches the maximum value of 779.43 Oe when  $x = 0.1$ , which indicates that the sample prepared belongs to hard magnetic material. The coercivity can be enhanced by the single domain region of nanoparticles to promote crystal growth. The high coercivity of MCNF is mainly attributed to the high magnetic anisotropy of Co<sup>2+</sup> at the B site of octahedron and its spin–orbit coupling. In addition, there are many factors affecting coercivity, such as spin tilt and lattice distortion, which can lead to coercivity changes [42].

In magnetic materials, spontaneous magnetization mainly comes from the isotropic exchange between spins. When there is no additional interaction in the crystal, the direction of spontaneous magnetization can be arbitrary, and the internal energy of the system does not change at this time. In practice, the direction of spontaneous magnetization of magnetic materials is always unique or in several specific normal directions, which is called the easy axis direction. Only when the external magnetic field is applied, the direction of magnetization can be turned from the easy axis direction; this phenomenon is called magnetocrystalline anisotropy. The magnetocrystalline anisotropy constant indicates the strength of anisotropy of the magnet. According to Table 4, the net magnetic moment and magnetocrystalline anisotropy decreased with the increases in La<sup>3+</sup> contents and increased when  $x = 0.1$ . The decreases in the net magnetic moment are due to the substitution of Fe<sup>3+</sup> ions by the non-magnetic La<sup>3+</sup> ions.

The field correlation of dM/dH (magnetization) curves at 300 K can also be used to understand the single-domain and multi-domain characteristics of crystals. Figure 10 shows

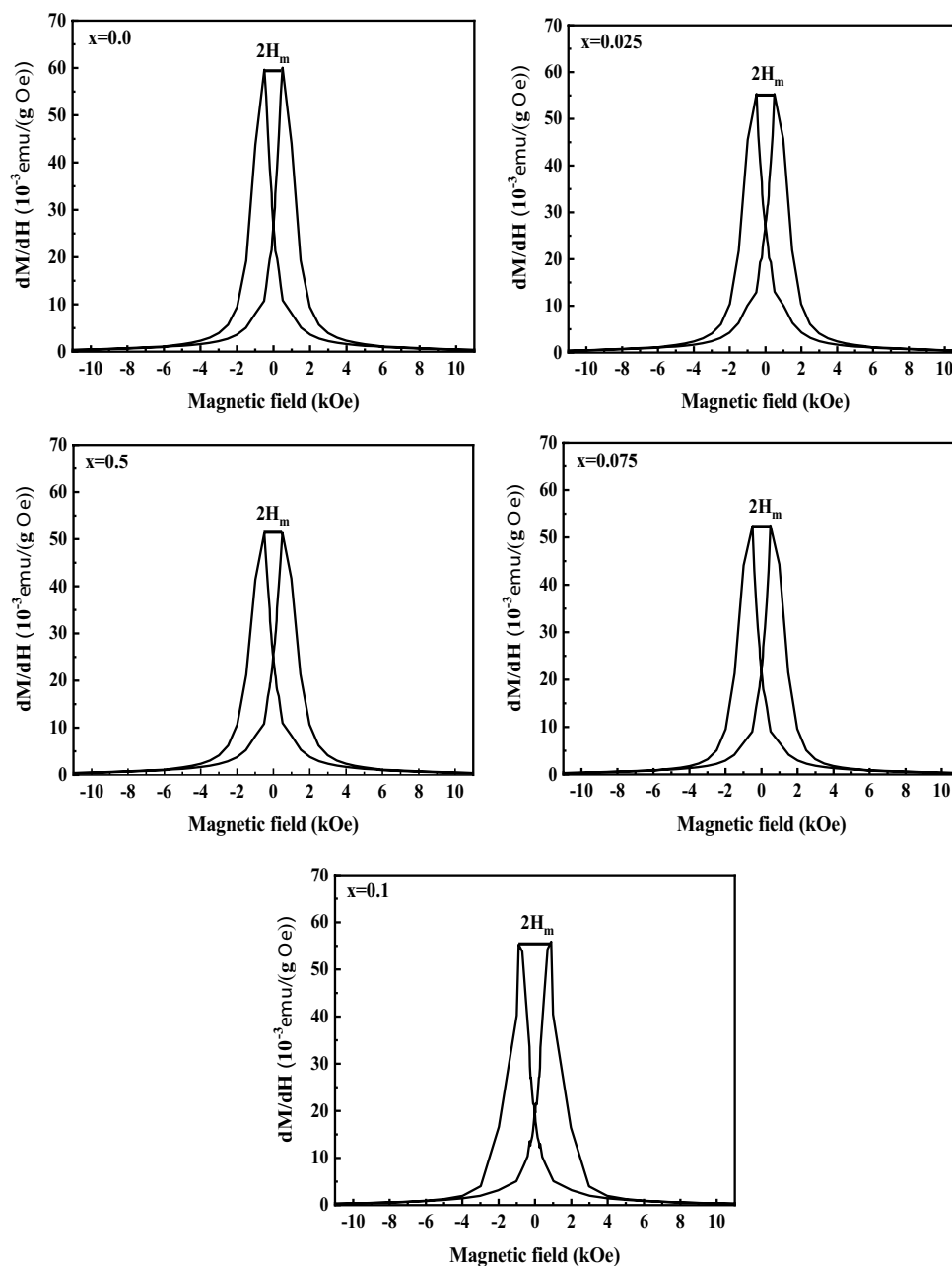
the magnetization ( $\chi$ ) plots with different doping amounts of La<sup>3+</sup> ions. As can be seen from the figure, the graph of 2Hm is symmetric at H = 0. According to the data in Table 4, when  $H \rightarrow 0$  and  $H \rightarrow H_m$ , the magnetization ( $\chi$ ) values are different, which indicates that La<sup>3+</sup>-doped MCNF have grain states of single domain, multiple domain and pseudo single domain. In addition, the increase in dM/dH peak value at Hm also indicates that the sample is magnetic stable to the ferrite with good spinel crystal structure.

## 4 Conclusions

Mg<sub>0.2</sub>Co<sub>0.8</sub>Fe<sub>2-x</sub>La<sub>x</sub>O<sub>4</sub> ( $x = 0, 0.025, 0.05, 0.075, 0.1$ ) were prepared by sol–gel method using citric acid as complexing agent. In the experiment, the sample's reaction process is complete, and no other impurity elements appeared. The samples were characterized and analyzed by XRD, FTIR, SEM, EDS and VSM. They are confirmed that the samples have spinel structures. By analyzing the crystal structure parameters such as lattice constant, average grain size and dislocation line density, it is concluded that most of La<sup>3+</sup> ions have replaced Fe<sup>3+</sup> ions, and the cations are redistributed, thus the structure has changed. In addition, the samples were spherical and formed magnetic clusters with narrow particle size distribution and uniform size. The samples have relatively high coercivity and high magnetization strength, which belongs to hard magnetic materials. Through the analysis of magnetic properties and magnetization curves, the samples have single domain, multiple domain and pseudo-single domain states.

The magnetic properties of the sample gradually increased with the increase in doping amount. The best magnetic properties appear when doping amount  $x = 0.1$ . However, the magnetic properties of the sample cannot reach

**Fig. 10** Field dependence of  $dM/dH$  of different samples.  $2H_m$  measures the magnetic field that separates two peaks



the ideal state. Therefore, the magnetic properties of samples under such doping can be improved by changing the pH value, drying temperature, sintering temperature or annealing temperature in the experimental process in the future.

## References

1. M.F. Huq, D.K. Sah, R. Ahmed, Z.H. Mahmood, Ni–Cu–Zn ferrite research: a brief review. *J. Sci. Res.* **216**, 215–233 (2013)
2. B. Coehi-Eromosele, S. Eejiweala, Palanawe, Magneto-structural properties of Ni–Zn nanoferrites synthesized by the low-temperature auto-combustion method. *B. Mater. Sci.* **1465**, 1465–1472 (2015)
3. P. Thakura, R. Sharma, M. Kumar, S.C. Katyal, P.B. Barman, V. Sharma, P. Sharma, Structural, morphological, magnetic and optical study of co-precipitated  $Nd^{3+}$  doped Mn–Zn ferrite nanoparticles. *J. Magn. Magn. Mater.* **317**, 317–325 (2019)
4. P.V. Gaikwad, R.J. Kamble, S.J. Mane-Gavade, S.R. Sabale, P.D. Kamble, Magneto-structural properties and photocatalytic performance of sol–gel synthesized cobalt substituted Ni–Cu ferrites for degradation of methylene blue under sunlight. *Physica B.* **79**, 79–85 (2019)
5. N. Feltin, M.P. Pileni, New Technique for Synthesizing Iron Ferrite Magnetic Nanosized Particles. *Langmuir* **3927**, 3927–3933 (1997)
6. W. Wernsdorfer, E. Bonet Orozco, K. Hasselbach, A. Benoit, D. Maily, O. Kubo, H. Nakano, B. Barbara, Macroscopic quantum

- tunneling of magnetization of single ferrimagnetic nanoparticles of barium ferrite. *Phys. Rev. Lett.* **4014**, 4014–4017 (1997)
7. K. Gwang-Hee, D.S. Hwang, Magnetic-field dependence of macroscopic quantum tunneling and coherence of ferromagnetic particles. *Phys. Rev. B* **55**, 8918–8917 (1997)
  8. Z. Ahmada, S. Atiqa, S. Kumail Abbasa, Shahid Mahmood Ramayb, Saira Riaza, Shahzad Naseem, Structural and complex impedance spectroscopic studies of Mg-substituted CoFe<sub>2</sub>O<sub>4</sub>. *Ceram. Int.* **1**, 0272–8842 (2016)
  9. C.O. Ehi-Eromosele, B.I. Ita, E.E.J. Iweala, Low-temperature combustion synthesis of cobalt magnesium ferrite magnetic nanoparticles: effects of fuel-to-oxidizer ratio and sintering temperature. *J. Sol-Gel Sci Techn.* **2**, 0928–1707 (2015)
  10. S.F. Mansour, O.M. Hemed, S.I. El-Dek, B.I. Salem, Influence of La doping and synthesis method on the properties of CoFe<sub>2</sub>O<sub>4</sub> nanocrystals. *J. Magn. Mater.* **7**, 7–8 (2016)
  11. M.I.A. Abdel Maksoud, G.S. El-Sayyad, A. Abokhadra, L.I. Soliman, H.H. El-Bahnasawy, A.H. Ashour, *J. Mater. Sci-Mater. El.* **2599**, 2598–2616 (2020)
  12. S.E. Jacobo, P.G. Bercoff, Structural and electromagnetic properties of yttrium-substituted Ni–Zn ferrites. *Ceram. Int.* **7664**, 7664–7668 (2016)
  13. R. Jasrotia, Virender Pratap Singh, Rajesh Kumar, Kirti Singha, Monika Chandel, Mahavir Singh, Analysis of Cd<sup>2+</sup> and In<sup>3+</sup> ions doping on microstructure, optical, magnetic and mössbauer spectral properties of sol-gel synthesized BaM hexagonal ferrite based nanomaterials. *Results Phys.* **1933**, 1933–1941 (2019)
  14. Muhammad Farooq Warsi, Ayesha Iftikhar, Muhammad Asif Yousuf, Muhammad Ilyas Sarwar, Sheraz Yousaf, Sajjad Haider, Mohamed F. Aly Aboud, Imran Shakir, Sonia Zulfiqar, Erbium substituted nickel–cobalt spinel ferrite nanoparticles: Tailoring the structural, magnetic and electrical parameters. *Ceram. Int.* **24194**, 24194–24203 (2020)
  15. S.M. Kabbur, U.R. Ghodake, R.C. Kambale, S.D. Sartale, L.P. Chikhale, S.S. Suryavanshi, Magnetic Electric and Optical Properties of Mg-Substituted Ni–Cu–Zn Ferrites. *J. Electron. Mater.* (2017). <https://doi.org/10.1007/s11664-017-5616-4>
  16. M.K. Shobana, Wonjong Nam, Heeman Choe, Yttrium-Doped Cobalt Nanoferrites Prepared by Sol-Gel Combustion Method and Its Characterization. *J. Nanosci. Nanotechnol.* **3535**, 3535–3538 (2013)
  17. Y. Xuan, Q. Li, G. Yang, Synthesis and magnetic properties of Mn–Zn ferrite nanoparticles. *J. Magn. Mater.* **464**, 464–469 (2007)
  18. M. Anis-ur-Rehman · MA Malik, M. Akram · M. Kamran · K Khan, A Maqsood, Structural and Magnetic Properties of Nanocrystalline Mg–Co Ferrites. *J. Supercond Nov Magn.* **2693**:2691–2696 (2012)
  19. Z.K. Heiba, M.B. Mohamed, A.M. Wahba, L. Arda, Magnetic and Structural Properties of Nanocrystalline Cobalt-Substituted Magnesium–Manganese Ferrite. *J. Supercond. Nov. Magn.* <https://doi.org/10.1007/s10948-015-3069-7> (2015)
  20. L.-Z. Li, X.-X. Zhong, R. Wang, Tu. Xiao-Qiang, L. Peng, Structural and magnetic properties of Co-substituted NiCu ferrite nanoparticles. *J. Magn. Mater.* **98**, 98–103 (2017)
  21. B. Rajesh Babu, M.S.R. Prasad, K.V. Ramesh, Y. Purushotham, Structural and Magnetic properties of Ni<sub>0.5</sub>Zn<sub>0.5</sub>Al<sub>x</sub>Fe<sub>2-x</sub>O<sub>4</sub> nano ferrite system. *Mater. Chem. Phys.* **586**, 585–591 (2014)
  22. S. Karimi, P. Kameli, H. Ahmadvand, H. Salamati, Effects of Zn–Cr-substitution on the structural and magnetic properties of Ni<sub>1-x</sub>Zn<sub>x</sub>Fe<sub>2-x</sub>Cr<sub>x</sub>O<sub>4</sub> ferrites. *Ceram. Int.* **16948**, 16948–16955 (2016)
  23. N. Yadav, A. Kumar, P.S. Rana, D.S. Rana, M. Arora, R.P. Pant, Finite size effect on Sm<sup>3+</sup>doped Mn<sub>0.5</sub>Zn<sub>0.5</sub>Sm<sub>x</sub>Fe<sub>2-x</sub>O<sub>4</sub> (0 ≤ x ≤ 0.5) ferrite nanoparticles. *Ceram. Int.* **8623**, 8623–8629 (2015)
  24. A.B. Gadkari, T.J. Shinde, P.N. Vasambekar, Structural analysis of Sm<sup>3+</sup>doped nanocrystalline Mg–Cd ferrites prepared by oxalate co-precipitation method. *Mater. Charact.* **1328**, 1328–1333 (2008)
  25. L. Wang, B.K. Rai, S.R. Mishra, Structural and magnetic study of Al<sup>3+</sup>doped Ni<sub>0.75</sub>Zn<sub>0.25</sub>Fe<sub>2-x</sub>Al<sub>x</sub>O<sub>4</sub> nanoferrites. *Mater. Res. Bull.* **813**, 183–194 (2015)
  26. A.M. Roy, Formation and stability of nanosized, undercooled propagating intermediate melt during β→δ phase transformation in HMX nanocrystal. **1**, 56001 (2021)
  27. A.M. Roy, Energetics and kinematics of undercooled nonequilibrium interfacial molten layer in cyclotetramethylene-tetranitramine crystal. *Physica B.* **1**, 412986 (2021)
  28. W.R. Agami, Effect of neodymium substitution on the electric and dielectric properties of Mn–Ni–Zn ferrite. *Physica B.* **534**, 17–21 (2018)
  29. M. Rahimi-Nasrabadi, M. Behpour, A. Sobhani-Nasab, S.M. Hosseinpour-Mashkani, ZnFe<sub>2-x</sub>La<sub>x</sub>O<sub>4</sub> nanostructure: synthesis, characterization, and its magnetic properties. *J. Multidiscip. Sci.* **26**, 9776–9781 (2015)
  30. N.S. Kumar, K.V. Kumar, Synthesis and structural properties of bismuth doped cobalt nanoferrites prepared by sol-gel combustion method. *World* **5**, 140–151 (2015)
  31. W. Wang, Z. Ding, X. Zhao, S. Wu, F. Li, M. Yue, J. P. Liu, Microstructure and magnetic properties of MFe<sub>2</sub>O<sub>4</sub> (M = Co, Ni, and Mn) ferrite nanocrystals prepared using colloid mill and hydrothermal method. *J. Appl. Phys.* **117**, 17A328 (2015)
  32. N. Suo, A. Sun, Y. Zhang, Yu. Lichao, L. Shao, Z. Zuo, Magnetic transformation of Ni–Mg–Zn ferrite substituted by the Co<sup>2+</sup> ions from soft magnetic to hard magnetic. *J. Mater. Sci.* **2390**(32), 3286–3302 (2021)
  33. A.B. Gadkaria, T.J. Shinde, P.N. Vasambekar, Structural analysis of Y<sup>3+</sup>-doped Mg–Cd ferrites prepared by oxalate co-precipitation method. *Mater. Chem. Phys.* **508**, 505–510 (2009)
  34. L. Yu, A. Sun, N. Suo, Z. Zuo, X. Zhao, W. Zhang, Structural, morphological and magnetic properties of Ni–Cu–Co ferrites by the Sm<sup>3+</sup> ions substitution. *Mod. Phys. Lett. B.* **10**, 2050236 (2020)
  35. V. Vinayak, P.P. Khirade, S.D. Birajdar, D.B. Sable, K.M. Jadhav, Structural, Microstructural, and Magnetic Studies on Magnesium (Mg<sup>2+</sup>)-Substituted CoFe<sub>2</sub>O<sub>4</sub> Nanoparticles. *J. Supercond. Nov. Magn.* **1026**, 1025–1032 (2016)
  36. Mi. Yan, X. Peng, *Fundamentals of Magnetism and Magnetic Materials* (Zhejiang University Press, Zhejiang, 2006), p. 10
  37. S. Bhukal, T. Namgyal, S. Mor, S. Bansal, S. Singhal, Structural, electrical, optical and magnetic properties of chromium substituted Co–Zn nanoferrites Cu<sub>0.6</sub>Zn<sub>0.4</sub>Cr<sub>x</sub>Fe<sub>2-x</sub>O<sub>4</sub> (0 ≤ x ≤ 1.0) prepared via sol-gel Au-to-combustion method. *J. Mol. Struct.* **1012**, 12–167 (2012)
  38. P.A. Shaikh, R.C. Kambale, A.V. Rao, Y.D. Kolekar, Effect of Ni doping on structural and magnetic properties of Co<sub>1-x</sub>Ni<sub>x</sub>Fe<sub>1.9</sub>Mn<sub>0.1</sub>O<sub>4</sub>. *J. Magn. Mater.* **322**, 718–726 (2010)
  39. J.M.D. Coey, *Rare-Earth Iron Permanent Magnets*, vol. 45 (Oxford University Press, Oxford, 1996), p. 5526
  40. J.M.D. Coey, Rare earth-iron permanent magnets. *J. Cheminformatics.* **23** (2010)
  41. V. Chaudhari, S.E. Shirsath, M.L. Mane, R.H. Kadam, S.B. Shelke, D.R. Mane, Crystallographic, magnetic and electrical properties of Ni<sub>0.5</sub>Cu<sub>0.25</sub>Zn<sub>0.25</sub>La<sub>x</sub>Fe<sub>2-x</sub>O<sub>4</sub> nanoparticles fabricated by sol-gel method. *J. Alloy. Compd.* **549**, 213–220 (2013)
  42. R. Jasrotia, Virender Pratap Singh, Rajesh Kumar, Kirti Singha, Monika Chandel, Mahavir Singh, Analysis of Cd<sup>2+</sup> and In<sup>3+</sup> ions doping on microstructure, optical, magnetic and mössbauer spectral properties of sol-gel synthesized BaM hexagonal ferrite based nanomaterials. *Results Phys.* **1938**, 1933–1941 (2019)